



# Applied Mathematics and Nonlinear Sciences

<https://www.sciendo.com>

## Higher-Order Spectral Analysis of Stray Flux Signals for Faults Detection in Induction Motors

Miguel E. Iglesias Martínez<sup>1,2</sup>, Jose A. Antonino-Daviu<sup>3</sup>, Pedro Fernández de Córdoba<sup>2</sup>, J. Alberto Conejero<sup>2</sup> †

<sup>1</sup> Departamento de Telecomunicaciones, Universidad de Pinar del Río, Pinar del Río, Martí 270, CP 20100, Cuba

<sup>2</sup> Instituto Universitario de Matemática Pura y Aplicada, Universitat Politècnica de València, E46022 València, Spain

<sup>3</sup> Instituto de Tecnología Eléctrica, Universitat Politècnica de València, E46022 València Spain

---

### Submission Info

Communicated by Juan Luis García Guirao  
Received September 4th 2019  
Accepted September 30th 2019  
Available online March 31st 2020

---

### Abstract

This work is a review of current trends in the stray flux signal processing techniques applied to the diagnosis of electrical machines. Initially, a review of the most commonly used standard methods is performed in the diagnosis of failures in induction machines and using stray flux; and then specifically it is treated and performed the algorithms based on statistical analysis using cumulants and polyspectra. In addition, the theoretical foundations of the analyzed algorithms and examples applications are shown from the practical point of view where the benefits that processing can have using HOSA and its relationship with stray flux signal analysis, are illustrated.

---

**Keywords:** Cumulants; Higher-Order Spectra; Stray Flux; Faults Diagnosis.  
**AMS 2010 codes:** 60K30, 60G35.

---

## 1 Introduction

The monitoring and diagnosis of rotary electric machines have taken great importance in current applications of industry, aeronautics, and telecommunications, among other branches of science and technology. They have fostered the development of numerous methods to monitor and diagnose different types of failures in electric

---

† Corresponding author.

Email address: [aconejero@upv.es](mailto:aconejero@upv.es)

machines. These techniques have been designed to increase machines efficiency, safety, and performance, from the reliability and energy point of view [17, 32].

In principle, each one of these techniques are based on processing different signals that can be captured by sensors that measure parameters such as mechanical vibrations, stator current, acoustic signal, and stray flux. They let us monitor the condition of electric machines and detect numerous failures such as design and manufacture defects, improper ambient conditions, overload and over-speed, fatigue, stator insulation failure, bearing fault, broken rotor bar/end-ring detection, and air gap eccentricity [17]:

One of the most commonly used techniques is vibration analysis [10, 12, 58] and motor-current analysis or motor current signature analysis (MCSA) [35, 64, 65]. These techniques are based on the spectrum analysis using the Fourier transform for the detection of specific faults since the frequency spectrum shows numerous harmonics including the fundamental and the faults adjacent frequencies, that differ between faulty and healthy motors, because different electrical and mechanical faults generate different signatures [11, 13, 16].

On the other hand, there are other techniques based on the acoustic signal processing that emanates from the rotor noise [1, 12, 19]. Their goal is to identify and extract features of signals that correspond to faults [18]. For this purpose, techniques like the Fourier transform has been used to analyze the noise [43]. However, it presents the fundamental disadvantage that the power spectrum is not immune to noise. Other techniques applied to this identification are based on high-resolution spectral analysis, wavelet transforms [2, 36, 55], and empirical modes decomposition [12].

Relating to artificial intelligence-based methods for diagnosing failures [38], there are several works for failure classifications and pattern recognition. These works are differentiated in dissimilar methods of artificial intelligence such as artificial neural networks [5, 26, 41, 48, 49, 56] genetic algorithms [54, 69], support vector machines [4, 21, 39, 57, 59, 68], Bayesian classifiers [42, 44, 70].

In general, these methods are based on the initial information available to the system, in addition to learning the process that can be supervised or unsupervised, and extracting characteristics based on logical knowledge, using the stator current, vibration signals and sounds of the motor.

Furthermore, failure detection methods based on higher-order statistical analysis have been applied to vibration signals, by considering the information provided by cumulants and moments of orders greater than or equal to two, as well as the spatial information that extracted from the analysis of higher-order spectra such as the bispectrum [29, 30, 33, 34, 50, 63, 66]. In addition to statistical estimators such as variance, kurtosis and skewness, derived from the cumulants of second, third, and fourth orders respectively are performed.

At present, the treatment of failures in electric induction machines has taken a high boom in relation to the analysis of the stray flux signals for the detection of failures, see the recent review of Jiang et al. [32]. However, it is not considered based on the use of statistical analysis of cumulants nor High-Order Spectra Analysis (HOSA). Since HOSA-based techniques are immune to Gaussian probabilistic density function noise, the spectral properties of the signal are preserved. Therefore, HOSA-based analysis of stray flux signals can be potentially used for fault detection.

We focus on providing an update of the statistical analysis techniques based on cumulants and higher-order spectra applied to the diagnosis of failures using stray flux signals. The work is organized as follows: In Section II, we review existing fault diagnosis methods from stray flux signals. In Section III, we show the theoretical foundations of a statistical analysis based on high-order cumulants and polyspectra. The use of HOSA on stray flux signals for fault detection is shown in Section IV. Finally, we provide some conclusions and prospective lines for future work in this line.

## 2 Faults Detection Based on Stray Flux Analysis

The magnetic flux is measured by circular search coils and hall sensors, that are concentric with the shaft inside the machine. They generate a voltage proportional to the magnetic field generated by the flux. In addition to these sensors, other types of sensors based on optical fiber and radiofrequency have been already used [17, 20].

Recently, a smart sensor has been proposed to detect winding insulation failures based on reconfigurable FPGA technology and using artificial neural networks [67].

## 2.1 Stator Insulation Monitoring And Failure Detection

Stray flux has been proved to detect the stator winding insulation failure. The main difference for fault detection respect to the use of flow signals consists of the type of sensor to be used and the position where the measurement is taken. One way to detect this type of failure is by applying a load and not load test, that provides significant similarities, even if the stator current gives interesting diagnostic information only when the motor is loaded.

Considering power supply harmonics, it is possible to easily detect the stator winding faults in the low-frequency range of the flux spectrum. One of the most used methods to detect this type of failure is the time-frequency analysis based on the signal spectrogram since this analysis generates important amplitude components in specific harmonics [32].

## 2.2 Bearing Fault Detection

It is estimated that approximately 35-55 percent of all cases of failures in electrical machines are Bearing Fault Detection, so this type of failure is investigated very frequently in the monitoring and diagnosis of electrical machines. Approximately 40 percent of these are caused by the inappropriate use of lubricants. Some indicators that reveal that the nature of this type of failure lies in the increase in temperature and mechanical vibrations and the increase in the acoustic noise level generated by the machine [14, 24, 31]. Some experimental measurements were carried out using a current probe and by means of different flux probes, positioned in different positions [14, 23]. The comparison is conducted to find the main advantages which are the simplicity and the flexibility of the custom flux probe with its amplification and filtering stage depend on the relative position used for the experiments [47].

## 2.3 Air Gap Eccentricity Detection

Motor eccentricity failures are permissible up to 10 percent, and they do not have a significant influence on the characteristics of the motor and its useful life. However, a high level of eccentricity can cause a magnetic imbalance and therefore an increase in noise and vibrations [71]. Experimental results have revealed the potential of a simple search coil for the detection and the distinction of the accurate eccentricity nature even in the presence of similar mechanical faults [53]. Dynamic eccentricity produces low-frequency air gap flux components. However, they can be observed in stator current only under mixed eccentricity. Moreover, detection of dynamic eccentricity in stator current around the principal slot harmonic (PSH) is only useful for some combination of pole pairs and rotor slots [53, 61, 62].

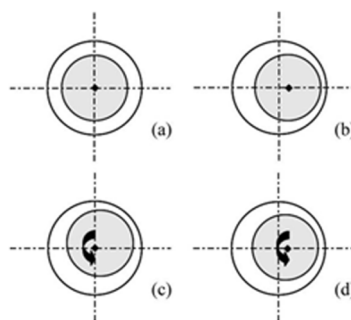


**Fig. 1** Examples of Eccentricity: a) Without eccentricity (b) Static eccentricity (c) Dynamic eccentricity (d) Mixed eccentricity. [47].

Under mixed eccentricity conditions, the stator currents contain the following frequencies [47]:

$$f_{ecc} = f \pm k(1-s)/pf, \quad (1)$$

where  $s$  is the machine slip. Since the frequencies related to the eccentricity and to the load torque overlap on the current sidebands, the frequencies provided by (1) are no longer enough for the diagnosis.

## 2.4 Broken Bars Detection

Induction motors are widely extended in industry, and among the defects which may appear, broken rotor bars represent 10 percent to 20 percent of the whole faults. This kind of failure does not cause an immediate breakdown, but it deteriorates the machine operation, decreasing its performance [7, 46]. For the detection of this type of failure, different algorithms based on the stray flux signal time-frequency analysis of the Fourier and wavelets transforms have been used. Each technique presents its particular advantages and drawbacks.

When a bar breakage occurs, a backward rotating magnetic field is generated due to the open-circuited bar. This creates an asymmetry in the rotor cage that is clearly reflected in the motors harmonic content [8, 15, 45]

The lower sideband harmonic leads to a torque (and speed) oscillation, which provokes the appearance of  $s$ , another harmonic in the stator current spectrum: the upper (or right) sideband harmonic given by  $1 + 2sf$ . Moreover, the frequency modulation on the rotational frequency  $f$ , provoked by the speed oscillation, also leads to sideband harmonics in the vibration (and, accordingly, in the noise) spectrum:

$$f_{bb} = f_{rr} \pm 2ksf \quad (2)$$

## 3 Higher-Order Statistical Analysis: Theoretical Foundations

Higher-order spectral analysis, also known as polyspectra, is defined in terms of higher-order statistics (cumulants, in particular). Among the specific cases of the higher-order spectra, we find the third-order spectrum, also called bispectrum or Fourier Transform of the third-order temporal cumulant, and the trispectrum or Fourier Transform of the fourth-order temporal cumulant Figure 2 illustrates the classification of the higher-order spectra of a signal. Although the higher-order statistical characteristics and the spectrum of a signal can be defined in terms of moments and cumulants, moments and their spectra can be very useful in the analysis of deterministic signals (transient and periodic), while cumulants and their spectra are of great importance in the analysis of stochastic signals [40].

There are several motivations behind the use of higher-order spectra in signal processing, which can be used to: (1) eliminate Gaussian additive colored noise from an unknown power spectrum; (2) extract information due to process deviations whose probabilistic distribution function is Gaussian, and (3) detect and characterize the nonlinear properties in the signals, as well as identify nonlinear systems.

The first motivation is based on the property that for stationary signals with Gaussian probabilistic distribution function, higher-order cumulants are equal to zero. If a non-Gaussian signal is received together with additive Gaussian noise, a calculation of the higher-order cumulant of the signal sample plus noise will eliminate the noise. Therefore, in these signal processing environments, there will be certain advantages for the detection and/or estimation of signal parameters through the cumulant of the observed data [40].

### 3.1 Higher-Order Statistics. Definition and Properties

In this section, the definitions, properties, and the way of calculating higher-order statistics are introduced. Let  $X = \{X(k)\}$ ,  $k = 0, \pm 1, \pm 2, \dots$  be a stationary random vector and its higher order moments exist, then:

$$m_n^X(\tau_1, \tau_2, \dots, \tau_{n-1}) = E\{X(k)X(k+\tau_1)\cdots X(k+\tau_{n-1})\} \quad (3)$$

where  $E$  denotes the expected value operator [6, 37, 40], represents the  $n$ -th order moment of  $X$ , which depends only on the different temporary displacements  $\tau_1, \tau_2, \dots, \tau_{n-1}$ , with  $\tau_i = 0, \pm 1, \dots$ . It can be seen that the second order moment  $m_2^X(\tau_1)$  is the autocorrelation function of  $X$ , likewise  $m_3^X(\tau_1)$  and  $m_4^X(\tau_1)$  represent the third and fourth order moments, respectively. The cumulants are similar to the moments, the difference is that the moments of a random process are derived from the characteristic function of the random variable, while the cumulant generating function is defined as the logarithm of the characteristic function of the random variable.

The  $n$ -th order cumulant of  $X$  can be written as, see [37]:

$$c_n^X(\tau_1, \dots, \tau_{n-1}) = m_n^X(\tau_1, \dots, \tau_{n-1}) - m_n^G(\tau_1, \dots, \tau_{n-1}), \quad n = 3, 4, \quad (4)$$

where  $m_n^G(\tau_1, \tau_2, \dots, \tau_{n-1})$  is the  $n$ -order moment of a process with equivalent Gaussian distribution. with the same average value and autocorrelation function as  $X$ , the stationary random vector. From (4) it is evident that for a process following a Gaussian distribution, the cumulants of order greater or equal than 2 are null, since  $m_n^X(\tau_1, \dots, \tau_{n-1})$  and  $m_n^G(\tau_1, \dots, \tau_{n-1})$  are null, too [25]

Although fourth-order cumulants imply a considerable increase in calculation complexity, they are especially necessary when third-order cumulants are canceled in the case of symmetrically distributed processes, such as uniform distributed processes from  $[-a, a]$ , with  $a \in \mathbb{R}$ , such as Laplace and Gaussian processes. Third-order cumulants are not canceled for processes whose probabilistic density function is not symmetric, such as exponential or Rayleigh processes, but can take extremely small values compared to the values presented by their fourth-order cumulants [60].

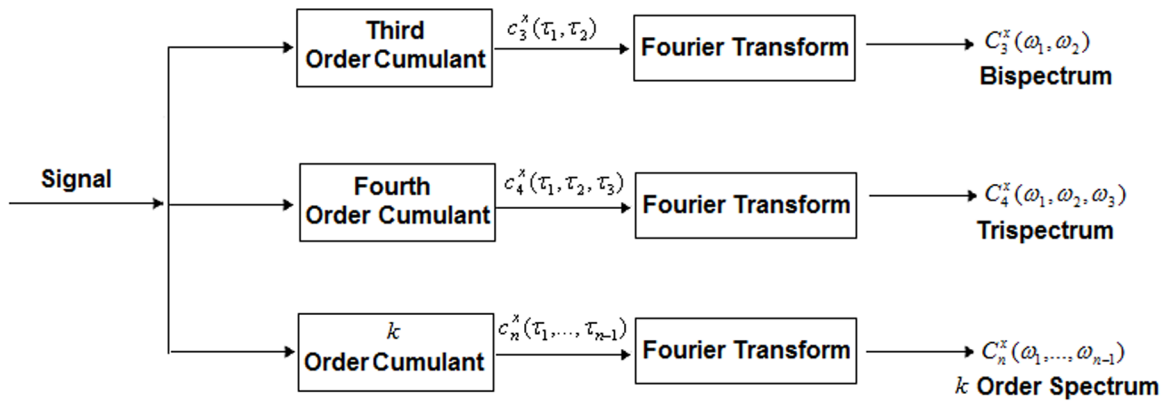


**Fig. 2** Higher-Order Spectral classification. Here,  $F_k(\cdot)$  denote the  $k$ -dimensional Fourier Transform, see [40].

### 3.2 Higher-Order Spectrum

The  $n$ -th order spectrum of a stationary random vector  $X = \{X(k)\}$ ,  $k = 0, \pm 1, \pm 2, \dots$  is defined as the multidimensional Fourier Transform  $F_k(\cdot)$  of order  $n - 1$  on the higher order statistical characteristics (moments and cumulants). The spectrum of the  $n$ -moment is defined as [25, 60]:

$$M_n^X(\omega_1, \dots, \omega_{n-1}) = F_n[m_n^X(\tau_1, \dots, \tau_{n-1})], \quad (5)$$

and, similarly, the spectrum of the  $n$ -cumulant is defined as

$$C_n^X(\omega_1, \dots, \omega_{n-1}) = F_n[mc_n^X(\tau_1, \dots, \tau_{n-1})], \quad (6)$$

Note that the spectrum of the  $n$ -th order cumulant is also periodic with period  $2\pi$ , that is:

$$C_n^X(\omega_1, \dots, \omega_{n-1}) = C_n^X(\omega_1 + 2\pi, \dots, \omega_{n-1} + 2\pi), \quad (7)$$

Equation expression also reads as:

$$C_n^X(\omega_1, \dots, \omega_{n-1}) = \frac{1}{(2\pi)^{n-1}} \sum_{\tau_1=-\infty}^{\infty} \dots \sum_{\tau_{n-1}=-\infty}^{\infty} c_n^X(\tau_1, \dots, \tau_{n-1}) e^{j(\omega_1 \tau_1 + \dots + \omega_{n-1} \tau_{n-1})} \quad (8)$$

In particular, for  $n = 2$  in (8), we have the *power spectrum*

$$C_2^X(\omega) = \frac{1}{2\pi} \sum_{\tau=-\infty}^{\infty} c_2^X(\tau) e^{-j\omega\tau}, \quad (9)$$

where  $|\omega| \leq \pi$  and  $c_2^X(\tau)$  represents the process covariance sequence, see [25, 60].

For  $n = 3$  in (8), we have the *bispectrum*

$$C_3^X(\omega_1, \omega_2) = \frac{1}{(2\pi)^2} \sum_{\tau_1=-\infty}^{\infty} \sum_{\tau_2=-\infty}^{\infty} c_3^X(\tau_1, \tau_2) e^{-j(\omega_1 \tau_1 + \omega_2 \tau_2)}, \quad (10)$$

where  $|\omega_1| \leq \pi$ ,  $|\omega_2| \leq \pi$ , and  $|\omega_1 + \omega_2| \leq \pi$  and  $c_3^X(\tau)$  represents the sequence of third order cumulants of  $X(k)$ . The expression of the cumulant complies with the following symmetric relationships [60]:

$$c_3^X(\tau_1, \tau_2) = c_3^X(\tau_2, \tau_1) = c_3^X(-\tau_2, \tau_1 - \tau_2) = c_3^X(\tau_2 - \tau_1, -\tau_1) \quad (11)$$

$$= c_3^X(\tau_1 - \tau_2, -\tau_2) = c_3^X(-\tau_1, \tau_2 - \tau_1) = c_3^X(\tau_1, \tau_2) \quad (12)$$

From these relationships, we can get a division of the plane  $\tau_1 \tau_2$  in six regions and, consequently, upon knowing the third-order cumulant in any of these six regions (see Figure 3), we can reconstruct the complete sequence corresponding to the third-order cumulants. Note that each one of these regions contains its border. Thus, for example, sector I is an infinite region characterized by  $0 \leq \tau_2 \leq \tau_1$ . For non-stationary processes, these six regions of symmetry disappear. From these relationships and the definition of the spectrum of third-order cumulants, the following relationships in the two-dimensional frequency domain can be obtained [6, 25, 37]

$$C_3^X(\omega_1, \omega_2) = C_3^X(\omega_2, \omega_1) = C_3^X(-\omega_2, -\omega_1) = C_3^X(-\omega_1 - \omega_2, \omega_2) \quad (13)$$

$$= C_3^X(\omega_1, -\omega_1 - \omega_2) = C_3^X(-\omega_1 - \omega_2, \omega_1) = C_3^X(\omega_2, \omega_1 - \omega_2) \quad (14)$$

Figure 3(b) shows the 12 symmetry regions of the bispectrum when real stochastic processes are considered and, similar to the temporal domain, the knowledge of the bispectrum in the triangular region It is enough for a total reconstruction of the bispectrum. Note that, in the frequency domain, the symmetry regions have a finite area and in general, the bispectrum takes complex values and, consequently, the phase information is preserved [60].

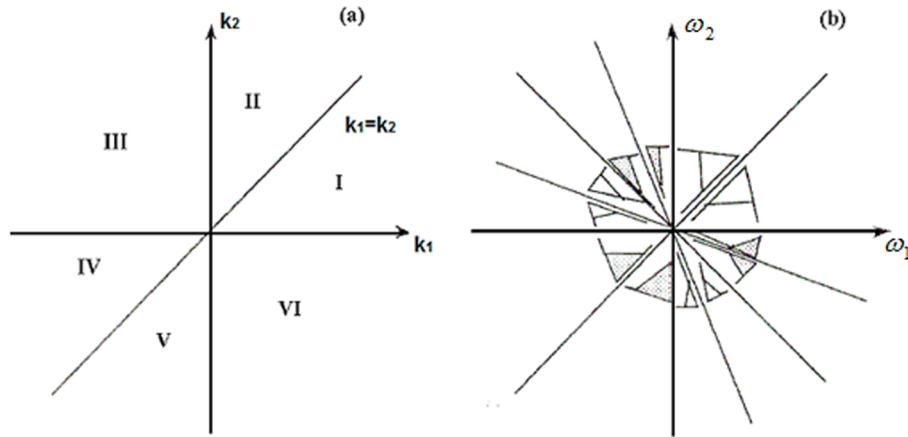


**Fig. 3** Symmetry regions for (a) the third-order cumulant and for (b) the bispectrum.

In the case  $n = 4$ , we get the *trispectrum*

$$C_4^X(\omega_1, \omega_2, \omega_3) = \frac{1}{(2\pi)^3} \sum_{\tau_1=-\infty}^{\infty} \sum_{\tau_2=-\infty}^{\infty} \sum_{\tau_3=-\infty}^{\infty} c_4^X(\tau_1, \tau_2, \tau_3) e^{-j(\omega_1 \tau_1 + \omega_2 \tau_2 + \omega_3 \tau_3)}, \quad (15)$$

where  $|\omega_1| \leq \pi, |\omega_2| \leq \pi, |\omega_3| \leq \pi$ , and  $|\omega_1 + \omega_2 + \omega_3| \leq \pi$ , where  $c_4^X(\tau_1, \tau_2, \tau_3)$  represents the sequence of fourth-order cumulants. By combining the definition of the trispectrum and the fourth-order cumulants, 96 regions of symmetry appear associated with a real process. From the spectra of higher-order cumulants, the expressions of their respective cumulants in the temporal domain can be retrieved, by applying the  $n$ -order inverse Fourier transform [60].

### 3.3 Examples of calculation of the Higher-Order Spectra

To illustrate in more detail the calculation of the higher-order spectra, we show several examples with periodic signals.

#### 3.3.1 Cosine signal

First, let us consider the cosine signal

$$X = A_k \cos(2\pi f_k t + \vartheta_k) \quad (16)$$

with amplitude  $A_k = 1$ , frequency  $f_k = 50\text{Hz}$ , and a phase  $\vartheta_k = 0$ , discretely generated from a sampling frequency of  $f_s = 1000\text{Hz}$  and a duration of 1024 samples. Then the bispectrum for a 1024 sample data window is equivalent to discretely performing the Fourier transform of the third order cumulant of the signal.

In figures 4 (a) and (b), respectively shows the cosine signal and its frequency spectrum using the one-dimensional Fourier Transform (FT). Likewise, as a comparison mode, the bispectrum of the 50 Hz cosine signal (0.05 normalized to 1) it is shown in Figure 5, to illustrate that the fundamental frequency of the signal prevails; and also showing other frequency components that by means of the one-dimensional spectrum using Fourier, they do not appear, which gives the bispectrum a higher resolution from the spectral point of view, which can be useful for dissimilar applications to find linear combinations or not, of existing relations between frequencies, for the development of identifying spectral patterns.

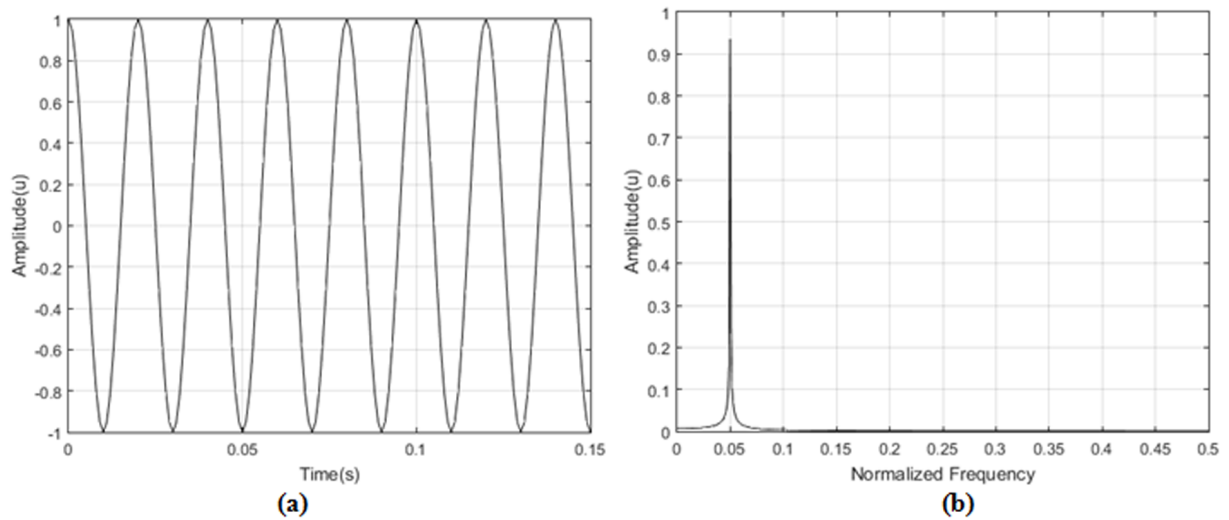


**Fig. 4** (a) A cosine signal of 50Hz (0.05 normalized frequency) and (b) its spectrum

Apart from the fundamental frequency component 0.05 (50Hz) normalized to 1, there are other components as results of linear combinations of the fundamental frequency (16), since the calculation of bispectrum results in a two-dimensional frequency and a phase matrix, see Figure 5.

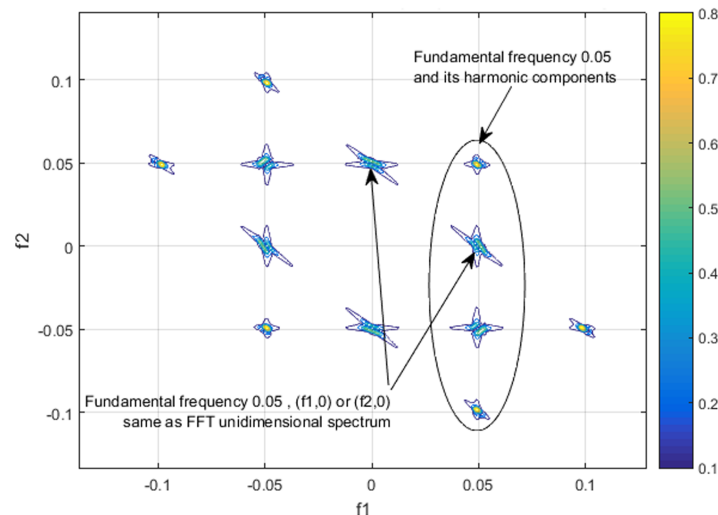


**Fig. 5** Contour plot of the bispectrum of the 50 Hz (0.05) cosine signal.

On the other hand, although less used, the phase spectrum of the cosine signal of (16) is also shown. The phase spectrum contains an arrangement with the amplitude in degrees of the phase of the signal, that is taken as  $\vartheta_k = \pi/4$  in (16). Its corresponding phase spectrum is shown below in Figure 6. We also show the phase bispectrum, see Figure 7, where the linear phase of the cosine signal is resalted in the bispectrum phase matrix.

The bispectrum preserves the phase information of every spectral component, that is the phase of the original signal and it can be obtained from the original signal as:

$$\vartheta_{C_3^X}(\omega_1, \omega_2) = \vartheta_X(\omega_1) + \vartheta_X(\omega_2) + \vartheta_X(\omega_1 + \omega_2) \tag{17}$$

where  $\vartheta_{C_3^X}(\omega_1, \omega_2)$  represents the phases matrix of every spectral component. This relation also permits to

retrieve the original phase of the signal.

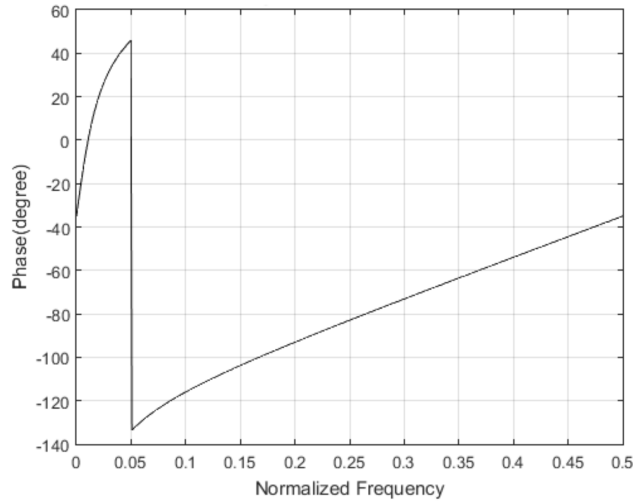


**Fig. 6** A phase spectrum of a cosine signal of 50Hz (0.05 normalized frequency)

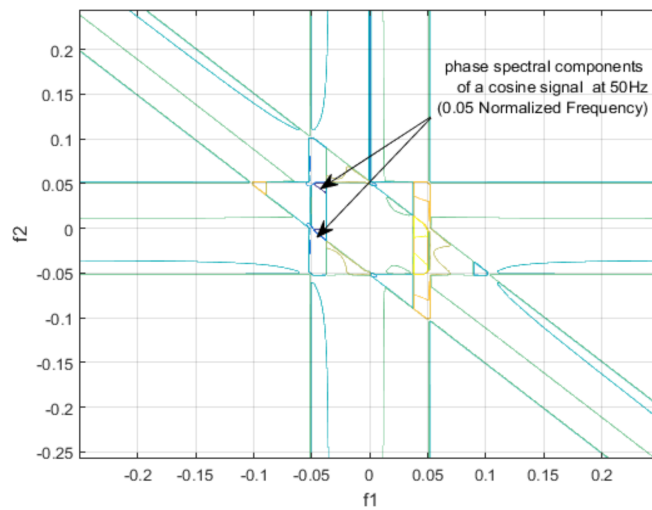


**Fig. 7** Contour plot of the phase bispectrum of a cosine signal of 50Hz (0.05 normalized frequency)

### 3.3.2 Harmonic signal

Secondly, we have also experimented by calculating the bispectrum of a harmonic signal of the form:

$$x(t) = A_k \cos(2\pi f_k + \vartheta_k) + 2A_k \cos(2\pi \cdot 3f_k + \vartheta_k) \tag{18}$$

In Figures 8 (a) and (b), we show the harmonic signal in time and its frequency spectrum using the one-dimensional Fourier Transform (FT). In Figure 9, the bispectrum of the harmonic signal is shown. We notice that the calculation of the bispectrum preserves the fundamental frequencies of each signal in the sum of harmonics, analogous to the calculation of the one-dimensional FT. We also observe that since the bispectrum is absolutely summable, multiple frequency components appear as a result of the linear combinations of the bispectrum of

both cosine signals individually.

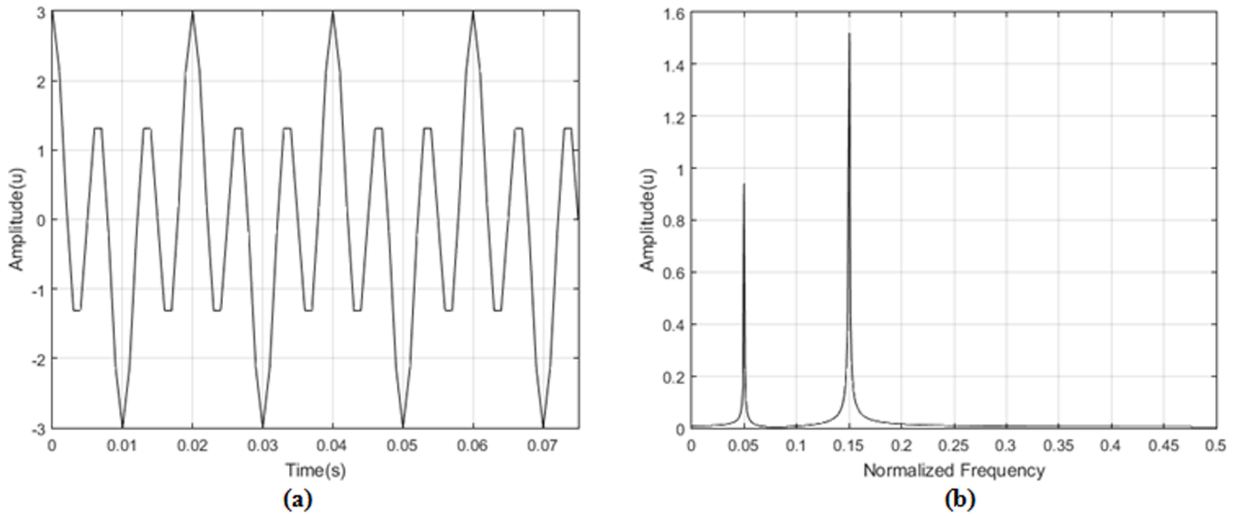


**Fig. 8** Illustration of : a) Harmonic Signal b) Harmonic Signal Spectrum

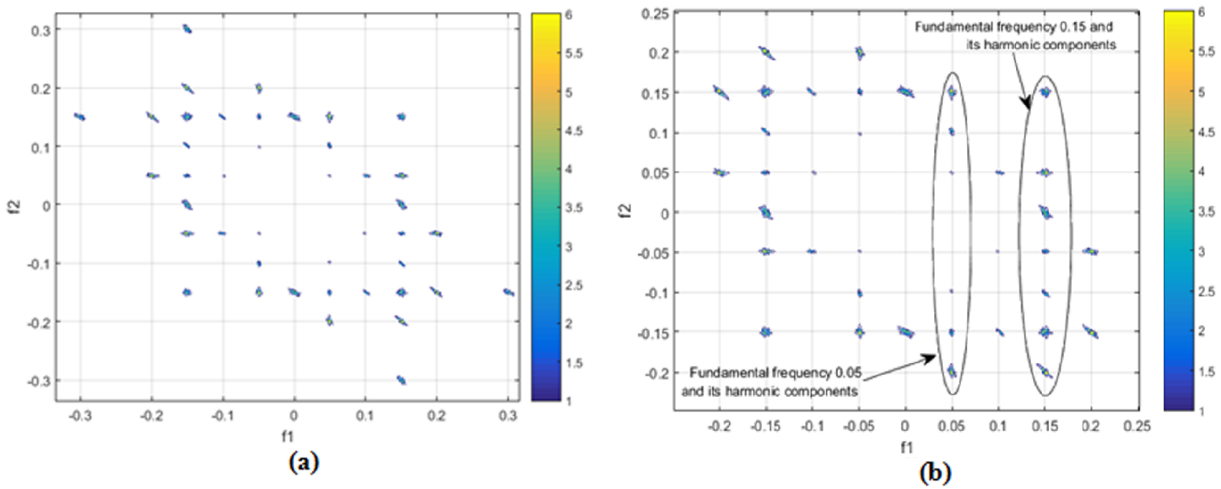


**Fig. 9** Contour Plot of: a) Bispectrum of the Harmonic Signal described in (14) and b) an expanded version of it.

We also show the phase bispectrum of the harmonic signal in Figure 10. It is more complex than the one of the cosine signal because the bispectrum is absolutely additive, and the phase of the 50Hz and 150Hz components are totally mixed.

#### 4 Using second and higher-order statistics with stray flux signals for faults detection

Although the analysis based on higher-order spectra in relation to the processing using the classical analysis based on the power spectrum can be advantageous, and the use of the stray flux signals is a non-invasive method, few works are linking HOSA (Higher-Order Statistic Analysis) and stray flux signals. This may be because computational complexity increases when using higher-order statistics in comparison to second-order statistics

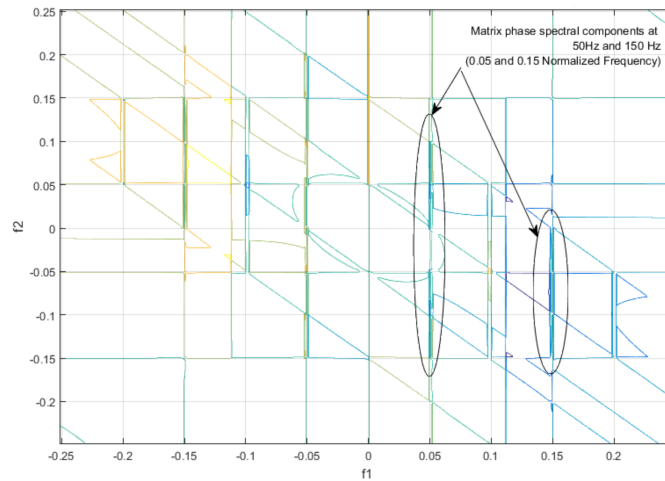


**Fig. 10** Contour plot of the phase bispectrum of a harmonic signal described in (14).

based on the Fourier one-dimensional transform. Most of the works based on the use of HOSA for diagnosing electric machines are based on the processing of vibration signals [3, 9, 22, 51, 52].

However, we have recently exposed the advantages of HOSA of stray flux signals [27], where an algorithm for the detection of the healthy-damaged state condition is proposed using temporary indicators in the frequency domain based on the bispectrum. Likewise, in [28], a second-order statistical analysis based on the autocorrelation function is linked with stray flux signals for the detection of non-adjacent bar breaks.

## 5 Conclusions

This work has shown a review of the techniques of processing and diagnosing of failures in electric induction machines. In particular, we have reported how to use them with flux signals. The theoretical foundations and with practical examples of the High-order statistical analysis (HOSA) and its potential for detecting failures in electrical machines have also been shown. On the other hand, validated results are also shown in references, of their use, using stray flux signals, which demonstrates that the linking of high-order statistical analysis techniques with the detection of failures in electric machines can be a very useful tool.

## Acknowledgements

This work has been supported by *Generalitat Valenciana, Conselleria d'Educació, Cultura i Esport* in the framework of the “*Programa para la promoción de la investigación científica, el desarrollo tecnológico y la innovación en la Comunitat Valenciana*”, Subvenciones para grupos de investigación consolidables (ref: AICO/2019/224). J. Alberto Conejero is also partially supported by MEC Project MTM2016-75963-P.

## References

- [1] H. Akçay and E. Germen. Subspace-based identification of acoustic noise spectra in induction motors. *IEEE Transactions on Energy Conversion*, 30(1):32–40, 2015.
- [2] J. Antonino-Daviu, M. Riera-Guasp, J. Roger-Folch, F. Martínez-Giménez, and A. Peris. Application and optimization of the discrete wavelet transform for the detection of broken rotor bars in induction machines. *Applied and Computational Harmonic Analysis*, 21(2):268–279, 2006.
- [3] N. Arthur and J. Penman. Induction machine condition monitoring with higher order spectra. *IEEE Transactions on Industrial Electronics*, 47(5):1031–1041, 2000.

- [4] T. P. Banerjee and S. Das. Multi-sensor data fusion using support vector machine for motor fault detection. *Information Sciences*, 217:96–107, 2012.
- [5] G. Bin, J. Gao, X. Li, and B. Dhillon. Early fault diagnosis of rotating machinery based on wavelet packets—empirical mode decomposition feature extraction and neural network. *Mechanical Systems and Signal Processing*, 27:696–711, 2012.
- [6] B. Boashash, E. J. Powers, and A. M. Zoubir. *Higher-order statistical signal processing*. Longman Cheshire, 1995.
- [7] A. Ceban, R. Pusca, and R. Romary. Eccentricity and broken rotor bars faults-effects on the external axial field. In *The XIX International Conference on Electrical Machines-ICEM 2010*, pages 1–6. IEEE, 2010.
- [8] I. Chernyavska and O. Vitek. Analysis of broken rotor bar fault in a squirrel-cage induction motor by means of stator current and stray flux measurement. In *2016 IEEE International Power Electronics and Motion Control Conference (PEMC)*, pages 532–537. IEEE, 2016.
- [9] T. Chow and G. Fei. Three phase induction machines asymmetrical faults identification using bispectrum. *IEEE Transactions on Energy Conversion*, 10(4):688–693, 1995.
- [10] X. Dai and Z. Gao. From model, signal to knowledge: A data-driven perspective of fault detection and diagnosis. *IEEE Transactions on Industrial Informatics*, 9(4):2226–2238, 2013.
- [11] J. de Jesus Rangel-Magdaleno, H. Peregrina-Barreto, J. M. Ramirez-Cortes, P. Gomez-Gil, and R. Morales-Caporal. Fpga-based broken bars detection on induction motors under different load using motor current signature analysis and mathematical morphology. *IEEE Transactions on Instrumentation and Measurement*, 63(5):1032–1040, 2013.
- [12] P. A. Delgado-Arredondo, D. Morinigo-Sotelo, R. A. Osornio-Rios, J. G. Avina-Cervantes, H. Rostro-Gonzalez, and R. de Jesus Romero-Troncoso. Methodology for fault detection in induction motors via sound and vibration signals. *Mechanical Systems and Signal Processing*, 83:568–589, 2017.
- [13] M. Drif and A. J. M. Cardoso. Stator fault diagnostics in squirrel cage three-phase induction motor drives using the instantaneous active and reactive power signature analyses. *IEEE Transactions on Industrial Informatics*, 10(2):1348–1360, 2014.
- [14] L. Frosini, C. Harlişca, and L. Szabó. Induction machine bearing fault detection by means of statistical processing of the stray flux measurement. *IEEE Transactions on Industrial Electronics*, 62(3):1846–1854, 2014.
- [15] Z. Gao, C. Cecati, and S. X. Ding. A survey of fault diagnosis and fault-tolerant techniques—part i: Fault diagnosis with model-based and signal-based approaches. *IEEE Transactions on Industrial Electronics*, 62(6):3757–3767, 2015.
- [16] M. Geethanjali and H. Ramadoss. Fault diagnosis of induction motors using motor current signature analysis: A review. In *Advanced Condition Monitoring and Fault Diagnosis of Electric Machines*, pages 1–37. IGI Global, 2019.
- [17] T. Ghanbari and A. Farjah. A magnetic leakage flux-based approach for fault diagnosis in electrical machines. *IEEE Sensors Journal*, 14(9):2981–2988, 2014.
- [18] A. Glowacz. Acoustic based fault diagnosis of three-phase induction motor. *Applied Acoustics*, 137:82–89, 2018.
- [19] A. Glowacz, W. Glowacz, Z. Glowacz, and J. Kozik. Early fault diagnosis of bearing and stator faults of the single-phase induction motor using acoustic signals. *Measurement*, 113:1–9, 2018.
- [20] T. Goktas, M. Zafarani, K. W. Lee, B. Akin, and T. Sculley. Comprehensive analysis of magnet defect fault monitoring through leakage flux. *IEEE Transactions on Magnetics*, 53(4):1–10, 2016.
- [21] K. C. Gryllias and I. A. Antoniadis. A support vector machine approach based on physical model training for rolling element bearing fault detection in industrial environments. *Engineering Applications of Artificial Intelligence*, 25(2):326–344, 2012.
- [22] F. Gu, Y. Shao, N. Hu, A. Naid, and A. Ball. Electrical motor current signal analysis using a modified bispectrum for fault diagnosis of downstream mechanical equipment. *Mechanical Systems and Signal Processing*, 25(1):360–372, 2011.
- [23] C. Harlişca, L. Szabó, L. Frosini, and A. Albini. Diagnosis of rolling bearings faults in electric machines through stray magnetic flux monitoring. In *2013 8TH International Symposium on Advanced Topics in Electrical Engineering (Atee)*, pages 1–6. IEEE, 2013.
- [24] R. Hoppler and R. A. Errath. Motor bearings, not must a piece of metal. In *2007 IEEE Cement Industry Technical Conference Record*, pages 214–233. IEEE, 2007.
- [25] R. M. Howard. *Principles of random signal analysis and low noise design: The power spectral density and its applications*. John Wiley & Sons, 2004.
- [26] J.-N. Hwang and Y. H. Hu. *Handbook of neural network signal processing*. CRC press, 2001.
- [27] M. E. Iglesias-Martínez, J. A. Antonino-Daviu, P. Fernández de Córdoba, and J. A. Conejero. Rotor fault detection in induction motors based on time-frequency analysis using the bispectrum and the autocovariance of stray flux signals. *Energies*, 12(4):597, 2019.
- [28] M. E. Iglesias-Martínez, P. F. de Cordoba, J. Antonino-Daviu, and J. A. Conejero. Detection of nonadjacent rotor faults in induction motors via spectral subtraction and autocorrelation of stray flux signals. *IEEE Transactions on Industry Applications*, 55(5):4585–4594, 2019.
- [29] M. E. Iglesias-Martínez, P. F. de Córdoba, J. A. Antonino-Daviu, and J. A. Conejero. Detection of bar breakages in induction motor via spectral subtraction of stray flux signals. In *2018 XIII International Conference on Electrical*

- Machines (ICEM)*, pages 1796–1802. IEEE, 2018.
- [30] M. E. Iglesias-Martínez, P. F. de Córdoba, J. A. Antonino-Daviu, and J. A. Conejero. Detection of adjacent and non-adjacent bar breakages in induction motors via convolutional analysis of sound signals. *Preprint*, 2020.
- [31] F. Immovilli, A. Bellini, R. Rubini, and C. Tassoni. Diagnosis of bearing faults in induction machines by vibration or current signals: A critical comparison. *IEEE Transactions on Industry Applications*, 46(4):1350–1359, 2010.
- [32] C. Jiang, S. Li, and T. G. Habetler. A review of condition monitoring of induction motors based on stray flux. In *2017 IEEE Energy Conversion Congress and Exposition (ECCE)*, pages 5424–5430. IEEE, 2017.
- [33] L. Jiang, Y. Liu, X. Li, and S. Tang. Using bispectral distribution as a feature for rotating machinery fault diagnosis. *Measurement*, 44(7):1284–1292, 2011.
- [34] Q. Jiang and F. Chang. A novel rolling-element bearing faults classification method combines lower-order moment spectra and support vector machine. *Journal of Mechanical Science and Technology*, 33(4):1535–1543, 2019.
- [35] X. Jin and T. W. Chow. Anomaly detection of cooling fan and fault classification of induction motor using mahalanobis–taguchi system. *Expert Systems with Applications*, 40(15):5787–5795, 2013.
- [36] J. Jóźwik. Identification and monitoring of noise sources of CNC machine tools by acoustic holography methods. *Advances in Science and Technology Research Journal*, 10(30), 2016.
- [37] S. M. Kay. *Fundamentals of statistical signal processing*. Prentice Hall PTR, 1993.
- [38] R. Liu, B. Yang, E. Zio, and X. Chen. Artificial intelligence for fault diagnosis of rotating machinery: A review. *Mechanical Systems and Signal Processing*, 108:33–47, 2018.
- [39] Z. Liu, H. Cao, X. Chen, Z. He, and Z. Shen. Multi-fault classification based on wavelet svm with pso algorithm to analyze vibration signals from rolling element bearings. *Neurocomputing*, 99:399–410, 2013.
- [40] J. M. Mendel. Tutorial on higher-order statistics (spectra) in signal processing and system theory: Theoretical results and some applications. *Proceedings of the IEEE*, 79(3):278–305, 1991.
- [41] M. Mrugalski, M. Witczak, and J. Korbcz. Confidence estimation of the multi-layer perceptron and its application in fault detection systems. *Engineering Applications of Artificial Intelligence*, 21(6):895–906, 2008.
- [42] V. Muralidharan and V. Sugumaran. A comparative study of naïve bayes classifier and bayes net classifier for fault diagnosis of monoblock centrifugal pump using wavelet analysis. *Applied Soft Computing*, 12(8):2023–2029, 2012.
- [43] Y. Ono, Y. Onishi, T. Koshinaka, S. Takata, and O. Hoshuyama. Anomaly detection of motors with feature emphasis using only normal sounds. In *Acoustics, Speech and Signal Processing (ICASSP), 2013 IEEE International Conference on*, pages 2800–2804. IEEE, 2013.
- [44] R. H. C. Palácios, I. N. da Silva, A. Goedel, and W. F. Godoy. A comprehensive evaluation of intelligent classifiers for fault identification in three-phase induction motors. *Electric Power Systems Research*, 127:249–258, 2015.
- [45] P. Panagiotou, I. Arvanitakis, N. Lophitis, J. A. Antonino-Daviu, and K. N. Gyftakis. Analysis of stray flux spectral components in induction machines under rotor bar breakages at various locations. In *2018 XIII International Conference on Electrical Machines (ICEM)*, pages 2345–2351. IEEE, 2018.
- [46] P. A. Panagiotou, I. Arvanitakis, N. Lophitis, J. Antonino-Daviu, and K. N. Gyftakis. A new approach for broken rotor bar detection in induction motors using frequency extraction in stray flux signals. *IEEE Transactions on Industry Applications*, 2019.
- [47] K. Pandey, P. Zope, and S. Suralkar. Review on fault diagnosis in three-phase induction motor. *MEDHA–2012, Proceedings published by International Journal of Computer Applications (IJCA)*, 2012.
- [48] J. Rafiee, F. Arvani, A. Harifi, and M. Sadeghi. Intelligent condition monitoring of a gearbox using artificial neural network. *Mechanical systems and signal processing*, 21(4):1746–1754, 2007.
- [49] A. Sadeghian, Z. Ye, and B. Wu. Online detection of broken rotor bars in induction motors by wavelet packet decomposition and artificial neural networks. *IEEE Transactions on Instrumentation and Measurement*, 58(7):2253–2263, 2009.
- [50] L. Saidi, J. B. Ali, and F. Fnaiech. Application of higher order spectral features and support vector machines for bearing faults classification. *ISA transactions*, 54:193–206, 2015.
- [51] L. Saidi, F. Fnaiech, G. Capolino, and H. Henao. Stator current bi-spectrum patterns for induction machines multiple-faults detection. In *IECON 2012-38th Annual Conference on IEEE Industrial Electronics Society*, pages 5132–5137. IEEE, 2012.
- [52] L. Saidi, F. Fnaiech, H. Henao, G. Capolino, and G. Cirrincione. Diagnosis of broken-bars fault in induction machines using higher order spectral analysis. *ISA Transactions*, 52(1):140–148, 2013.
- [53] M. Salah, K. Bacha, and A. Chaari. An improved spectral analysis of the stray flux component for the detection of air-gap irregularities in squirrel cage motors. *ISA transactions*, 53(3):816–826, 2014.
- [54] B. Samanta. Gear fault detection using artificial neural networks and support vector machines with genetic algorithms. *Mechanical systems and signal processing*, 18(3):625–644, 2004.
- [55] P. Sangeetha and S. Hemamalini. Dyadic wavelet transform-based acoustic signal analysis for torque prediction of a three-phase induction motor. *IET Signal Processing*, 11(5):604–612, 2017.
- [56] J. Sanz, R. Perera, and C. Huerta. Gear dynamics monitoring using discrete wavelet transformation and multi-layer perceptron neural networks. *Applied Soft Computing*, 12(9):2867–2878, 2012.

- [57] Z. Shen, X. Chen, X. Zhang, and Z. He. A novel intelligent gear fault diagnosis model based on emd and multi-class tsvm. *Measurement*, 45(1):30–40, 2012.
- [58] A. Singhal and M. A. Khandekar. Bearing fault detection in induction motor using fast fourier transform. In *IEEE Int. Conf. on Advanced Research in Engineering & Technology*, 2013.
- [59] A. Soualhi, K. Medjaher, and N. Zerhouni. Bearing health monitoring based on hilbert–huang transform, support vector machine, and regression. *IEEE Transactions on Instrumentation and Measurement*, 64(1):52–62, 2014.
- [60] A. Swami, G. B. Giannakis, and G. Zhou. Bibliography on higher-order statistics. *Signal processing*, 60(1):65–126, 1997.
- [61] O. Vitek, M. Janda, and V. Hajek. Effects of eccentricity on external magnetic field of induction machine. In *Melecon 2010-2010 15th IEEE Mediterranean Electrotechnical Conference*, pages 939–943. IEEE, 2010.
- [62] H. Wang, X. Bao, C. Di, and Z. Cheng. Detection of eccentricity fault using slot leakage flux monitoring. In *2015 9th International Conference on Power Electronics and ECCE Asia (ICPE-ECCE Asia)*, pages 2188–2193. IEEE, 2015.
- [63] Y. Wang, J. Xiang, R. Markert, and M. Liang. Spectral kurtosis for fault detection, diagnosis and prognostics of rotating machines: A review with applications. *Mechanical Systems and Signal Processing*, 66:679–698, 2016.
- [64] Z. Wang and C. Chang. Online fault detection of induction motors using frequency domain independent components analysis. In *2011 IEEE International Symposium on Industrial Electronics*, pages 2132–2137. IEEE, 2011.
- [65] Z. Wang, C. Chang, and Y. Zhang. A feature based frequency domain analysis algorithm for fault detection of induction motors. In *2011 6th IEEE Conference on Industrial Electronics and Applications*, pages 27–32. IEEE, 2011.
- [66] W. Wenbing and X. Jinquan. The application of coupled three order cumulants’ differential feature in fault diagnosis. In *2017 International Conference on Virtual Reality and Visualization (ICVRV)*, pages 374–375. IEEE, 2017.
- [67] I. Zamudio-Ramirez, R. A. Osornio-Rios, M. Trejo-Hernandez, R. d. J. Romero-Troncoso, and J. A. Antonino-Daviu. Smart-sensors to estimate insulation health in induction motors via analysis of stray flux. *Energies*, 12(9):1658, 2019.
- [68] X. Zhang and J. Zhou. Multi-fault diagnosis for rolling element bearings based on ensemble empirical mode decomposition and optimized support vector machines. *Mechanical Systems and Signal Processing*, 41(1-2):127–140, 2013.
- [69] W. Zhao, T. Tao, and E. Zio. System reliability prediction by support vector regression with analytic selection and genetic algorithm parameters selection. *Applied Soft Computing*, 30:792–802, 2015.
- [70] W. Zhao, Y. Zhang, and Y. Zhu. Diagnosis for transformer faults based on combinatorial Bayes Network. In *2009 2nd International Congress on Image and Signal Processing*, pages 1–3. IEEE, 2009.
- [71] F. Zidat, J.-P. Lecoq, F. Morganti, J.-F. Brudny, T. Jacq, and F. Streiff. Non invasive sensors for monitoring the efficiency of ac electrical rotating machines. *Sensors*, 10(8):7874–7895, 2010.